analytical chemistry

pubs.acs.org/ac

Letter

Screened α-Helix Peptide Inhibitor toward SARS-CoV-2 by Blocking a Prion-like Domain in the Receptor Binding Domain

Shang Wu, Limin Zhang, and Weizhi Wang*

Cite This: https://doi.org/10.1021/acs.analchem.2c02223

Read Online

ACCESS | Metrics & More | Article Recommendations | Supporting Information

ABSTRACT: A new peptide inhibitor was designed and optimized from an α-helix-rich peptide library specifically toward the critical prion-like domain (PLD) of SARS-CoV-2. It compactly blocked the S1 protein and potently neutralized the pseudovirus which shows promising potential for prophylactic and treatment of COVID-19.

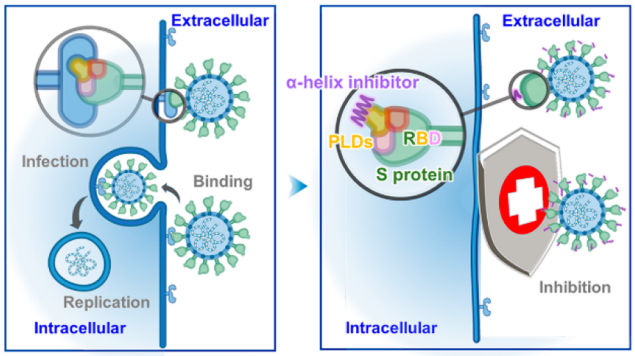

The pandemic of the coronavirus disease 2019 (COVID-19) wave has hit the world with unprecedented and calamitous intensity, which leads to a thorny medical emergency.[1] Although there are several enrolled vaccines in clinical use, specific medicine for prevention and treatment is in urgent demand. The structure proteins that incorporated into the severe acute respiratory syndrome coronavirus 2 (SARS-CoV-2) envelope lipid bilayer include spike (S), envelope (E), membrane (M), and nucleocapsid (N). Among them, the S protein could potently recognize and bind to the specific receptor, angiotensin converting enzyme 2 (ACE2), of the mammal host.[2,3] With the aid of various enzymes and cofactor proteins, such as transmembrane protease serines (TMPRSS2),[4] Mpro,[5] and FURIN,[6] SARS-CoV-2 finally enters into host cells. Therefore, it is feasible to design and construct neutralizing agents which could occlude those proteins, furthermore inhibiting the virus to infect host cells. At present, Paxlovid targeting Mpro[7] and Molnupiravir which act through the SARS-CoV-2 polymerase[8] were already enrolled in clinical studies. Among the above-mentioned proteins, intercepting the binding between the receptor binding domain (RBD) in the S protein and ACE2 is certainly a direct and effective way. On the other hand, delivering a high concentration of viral inhibitors into the nose could be a prospective auxiliary treatment because the SARS-CoV-2 infection generally begins in the nasal cavity.[9,10] Therefore, by virtue of low cost and extraordinary penetrability, developing small molecular neutralizing agents offers the possibility for intranasal delivery.[2,11] For instance, a series of DNA aptamers were screened and generated via capillary electrophoresis (CE)-based systematic evolution of ligands by the exponential enrichment (SELEX) method.[12] A series of humanized single-domain antibodies (sdAbs) were designed and selected from a synthetic library.[13,14] Peptides are also applicable, exhibiting a lower screening threshold thanks to the well-established technologies. Recently, several peptide sequences were designed and obtained via quartz crystal microbalance-based screening.[15]

However, things are far more complex than expected. With the remarkable success in the structural resolution of SARS-CoV, it was revealed that SARS-CoV-2 is the only coronavirus with a prion-like structural domain (PLD) distributed in the RBD. This structure is a set of low-complexity regions, rich in asparagine (Q) and glutamine (N) (e.g., Q474, Q493, Q498, N501, etc.),[16] which can interact with prion-like domains in the α1 helix of the ACE2 receptor (e.g., Q24, K353, Q42, etc.). This may explain why SARS-CoV-2 has a 10−20-fold higher affinity than SARS-CoV.[11,17] Therefore, the development of small molecular neutralizing agents targeting the PLD may have a higher blocking effect but faces greater challenges. Still, it should be noted that when peptides are too short, it is difficult for them to maintain a secondary structure, and they are unable to block the whole SARS-CoV-2 binding surface.[18] α-Helices, as mature and basic folding patterns, with their well-ordered secondary structures endowed peptides with stability and comprehensive binding ability, which supply a more reliable therapeutic strategy.[2]

Since the inhibitor-library-design strategy would center on the above-mentioned hot spots, the proper library-construction

Received: May 24, 2022
Accepted: July 7, 2022

Table 1. Peptide Affinities in SPRi Detection

name of peptides	amino acid sequence	S1 protein binding (SPR)		
		k_a (M^{-1} s^{-1})	k_d (s^{-1})	K_D (M)
W1	KIDRLKWKIAQLKADVDKLEADNAQLDA	3.63×10^4	5.34×10^{-4}	1.47×10^{-8}
W2	KIEKLKWKNAQLKADVDKLDAENAQLDA	2.03×10^4	2.54×10^{-4}	1.25×10^{-8}
W13	KVDKLKWKIATLKADVDKLDLENAQLDA	1.36×10^4	4.17×10^{-4}	3.06×10^{-8}
W25	KIDRLKWKVASLKADVDKLDAENAQLDA	1.39×10^4	4.23×10^{-4}	3.04×10^{-8}
W37	KVDRLRWRVATLRNEIDKLEVDNAQLDA	4.9×10^3	3.84×10^{-4}	7.85×10^{-8}
W71	KVDRLKWKIAQLKADVDKLEADNAQLDA	9.59×10^3	6.97×10^{-4}	7.27×10^{-8}

Scheme 1. Overview of the Inhibitor-Library-Design Strategy Aiming the PLD[a]

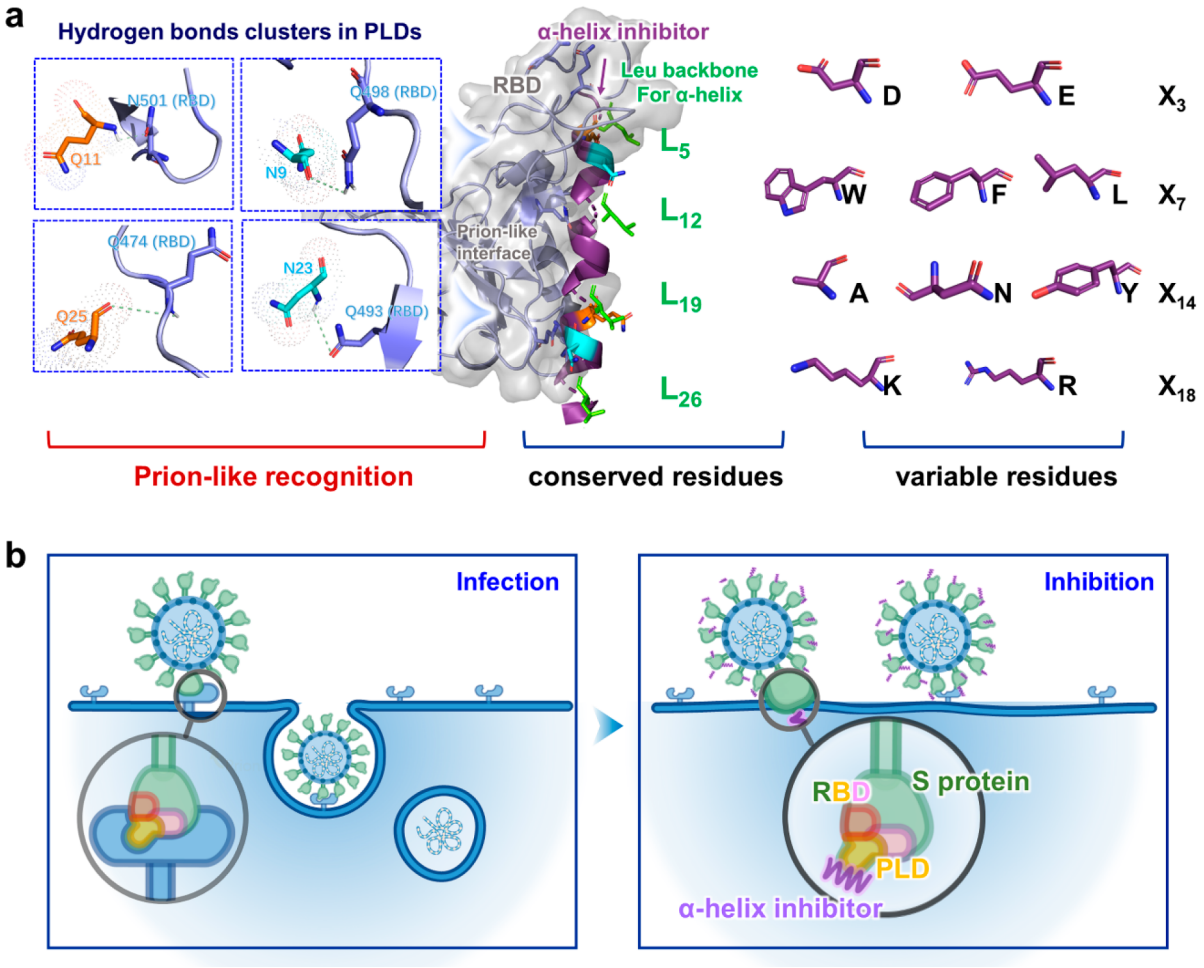

[a](a) Schematic of the interactions between the α-helix inhibitor (purple) and the SARS-CoV-2 RBD (deep blue), showing selected interacting side chains. The α-helix inhibitor consists of conserved residues including the Leu backbone (green) for α-helix formation inclination and Q (orange) and N (light blue) enriched areas for prion-like recognition and variable residues (purple) predominated by hydrophilic residues. (b) The α-helix peptide aimed at binding the PLD with the RBD furthermore inhibits SARS-CoV-2 from infecting host cells.

process is divided into three categories, α helix backbone, PLD, and variable residues. Herein, based on these goals, N_9, Q_{11}, N_{23}, and Q_{25} were fixed, which induced the PLD to emerge and emulated the α1 helix of ACE2 in favor of specifically binding the PLD of the RBD as two "falcula". L_5, L_{12}, L_{19}, and L_{26} were set as a backbone in tandem with the NAQLDA sequence underlying the α-helix inclination. Hydrophilic residues predominate among variable residues especially X_3, X_{15}, X_{17}, X_{20}, and X_{22} which are located at the opposite side of the L backbone and bring about an extensive hydrophilic interface. To testify as to the function of the PLD, a series of peptides whose N_9 and Q_{11} are replaced by other hydrophilic residues were added to the library as control groups. A library of over 10^7 synthetic peptides was designed fully compliant and screened by the microfluidic 'one-bead-one-compound (OBOC)' combinatorial chemistry approach finally yielding 71 distinctive peptides (Figure 1a) through the sequence alignment based on our previous works.[19,20] Those peptides were optimized in the next round via sorting the affinity demonstrated by surface plasmon resonance (SPR) detection. The K_D values of the selected potential peptide inhibitors, in turn, were 12.5, 14.7, 30.4, 30.6, 72.7, and 78.5 nM, respectively. As we expect, the peptide whose X_9 and X_{11} are N and Q exhibits an extraordinary binding affinity; besides, the

https://doi.org/10.1021/acs.analchem.2c02223
Anal. Chem. XXXX, XXX, XXX−XXX

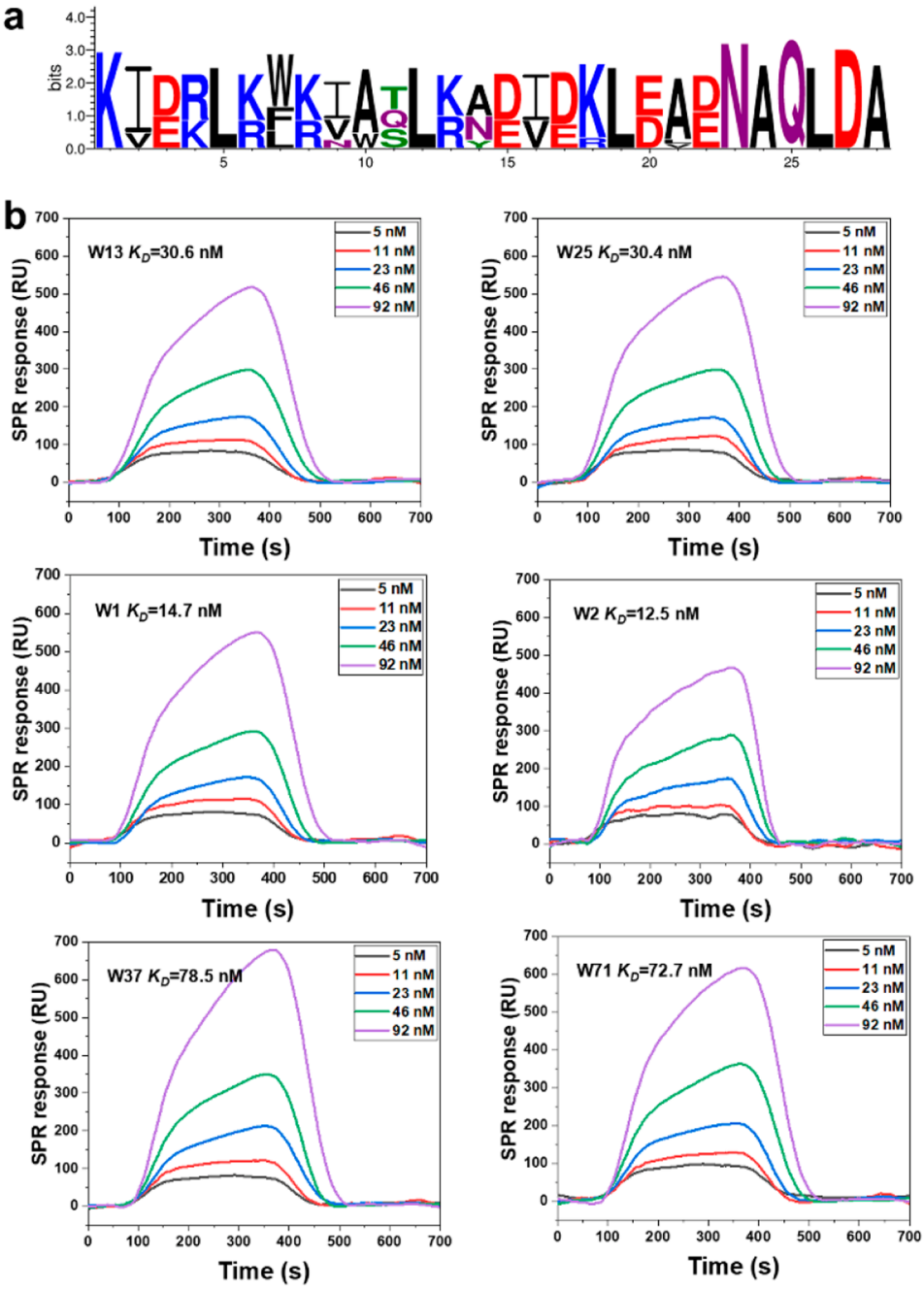

Figure 1. Selection strategy for identification of the W2 peptide that disrupts Spike-ACE2 interactions. (a) Alignment of the 71 screened peptide sequences generated by the Weblogo alignment tool. (b) Binding affinity of six potential peptides toward the SARS-CoV-2 S1 protein at different concentrations by SPRi detection.

peptide whose X_9 is fixed by N is also superior (Figure 1b and Table 1). The α-helix inhibitor with the highest affinity was named W2 and synthesized (Figure 2a). Circular dichroism (CD) indicated that W2 forms the α-helix structure (Figure 2c). To determine the possible binding sites, the SARS-CoV-2 S1 protein and the peptide were docked tentatively. The docking process was analyzed with PyMOL, demonstrating W2 could bind the RBD of the S1 protein appropriately (Figure 2b). To further redefine their position, the RBD and W2 were docked subsequently, indicating that the PLD of W2 can occupy the prion subsets of the RBD, and the binding sites for W2 and the RBD mainly include Asn_9-Gln_{498} (hydrogen bond), Gln_{11}-Asn_{501} (hydrogen bond), Asn_{23}-Gln_{493} (hydrogen bond), and Gln_{25}-Gln_{474} (hydrogen bond). Meanwhile, a hydrophilic interface was constructed between the variable residue of W2 and the subsets near the PLD, with binding free energy of −6.17 kcal/mol, which is consistent with the conserved sequences of our design (Scheme 1 and Figure 2b).

In order to quantify the neutralization activity of W2 peptides on the RBD, we carried out a bilateral competitive binding assay, in which the RBD has been precoated onto well plate strips, introducing the ACE2 protein to compete with the peptides. Indicated by horseradish peroxidase (HRP) and 3,3′,5,5′-tetramethylbenzidine (TMB), the reagent would be dimmer if the neutralizing agent occluded the RBD (Figure 2d). Inhibition activity was obtained by comparing with the

https://doi.org/10.1021/acs.analchem.2c02223
Anal. Chem. XXXX, XXX, XXX−XXX

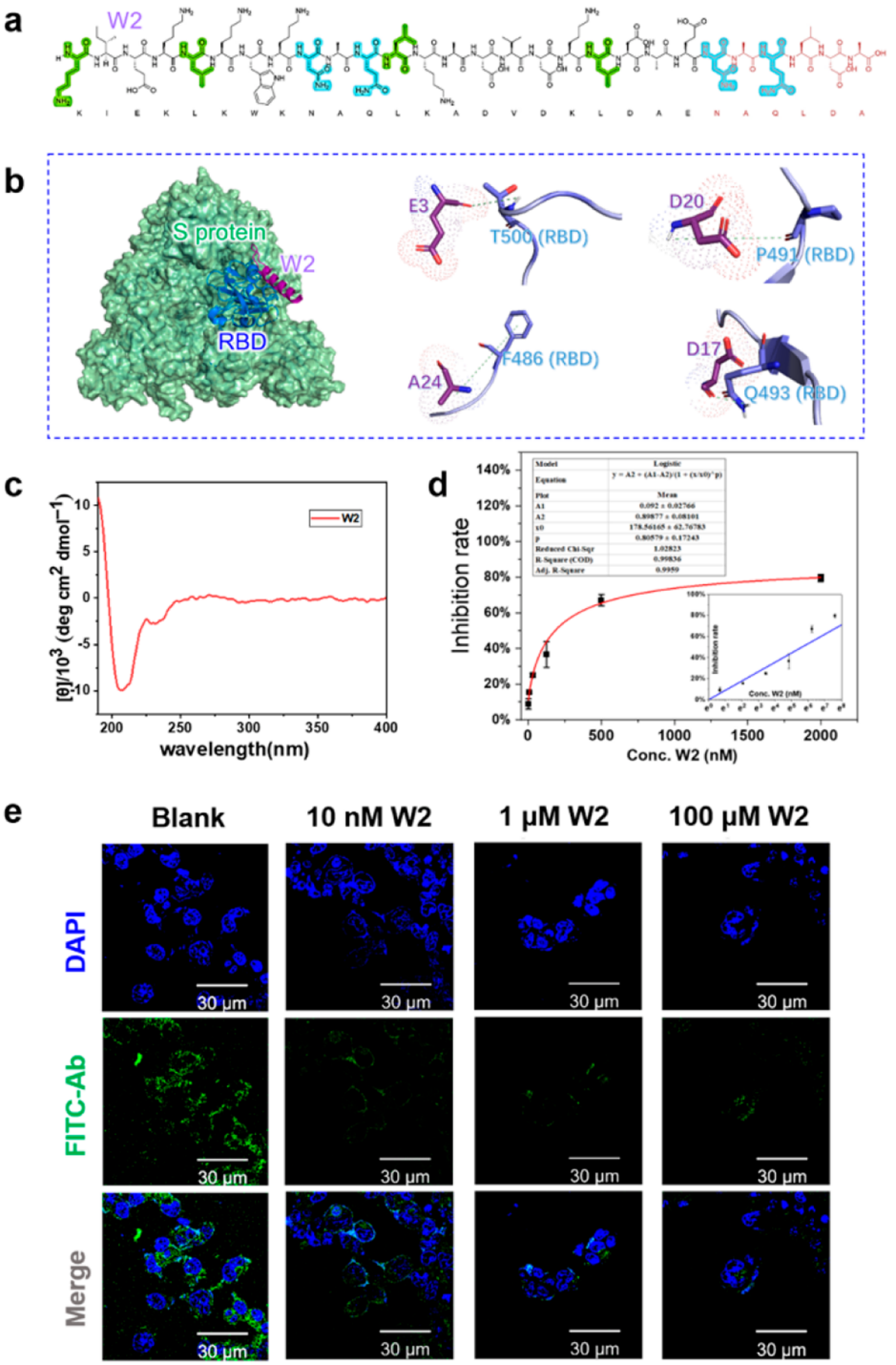

Figure 2. Inhibition ability of W2 toward the SARS-CoV-2 S1 protein and pseudovirus. (a) Molecular structure of W2. (b) Binding sites between W2 (purple) and the S1 protein (green), especially variable residues: E3-T500 (RBD), D17-Q493 (RBD), D20-P491 (RBD), and A24-F486 (RBD). (c) CD spectra of W2. Every value of the CD data used was the average of three scans and corrected for the background of W2 and the solvent. (d) Inhibition rate of W2 peptides against the RBD binding to ACE2 determined via the enzyme linked immunosorbent assay (ELISA), showing as linear-scale and ln-scale (inset). (e) Confocal laser scanning microscopy (CLSM) images of GFP expression. Dimmer GFP expression indicates the pseudovirus infection is inhibited by W2. Nuclei were stained by DAPI (blue). Scale bar, 30 μm.

negative control group. The results show the RBD hardly binds with ACE2 as the peptide concentration increases, with an IC_{50} of 196.82 nM, suggesting that the binding sites have been blocked by the peptides (Figure 2e). Stepping in at the cellular level, the HEK293-ACE2$^+$ cell stably overexpressing ACE2 was prepared as a host cell model. To testify and estimate the inhibitory effect of W2 when binding with the S1 protein on SARS-CoV-2, we next utilized the SARS-CoV-2 pseudovirus infection model which scattered the S protein on the surface. When the SARS-CoV-2 pseudovirus entered into host cells

https://doi.org/10.1021/acs.analchem.2c02223
Anal. Chem. XXXX, XXX, XXX−XXX

successfully, this model could express the green fluorescent protein (GFP) stably. The faded green fluorescent protein means that the SARS-CoV-2 pseudovirus has lost most of its power in the culture preincubated with W2 compared to the control group. Besides, the amount of luminous cells also decreased; with the addition of 1 μM W2, less than half of the host cells luminate, and as the dosage increases to 100 μM, almost no host cells luminate, according to a dose-dependent inhibition principle (Figure 2e and Supplementary Figure S5). Furthermore, to examine the cytotoxicity of the peptide on HEK293-ACE2$^+$ cells, we conducted the 3-(4,5)-dimethylthiahiazo(-z-y1)-3,5-diphenytetrazoliumromide (MTT) assay. HEK293-ACE2$^+$ cells were coincubated with 10 nM−100 μM W2 for 24 h, and the cell viability of the group was scarcely influenced, evincing that W2 has a reassuring safety profile at the cellular level (Supplementary Figure S3).

In this work, we offered a systematic design and screen strategy aiming the PLD for SARS-Cov-2. Based on this, peptide W2 stands out due to the high inhibition rate toward the S1 protein and the SARS-CoV-2 pseudovirus. To date, the PLDs in all variants of SARS-CoV-2 are relatively conserved,[16,21,22] whereupon the peptide has the potential to be a leading compound inhibitor with broad spectrum. In the future, the peptides should be tested in a living virus and in vivo. We will delve into it and hope to limit the increasing toll of the COVID-19 pandemic.

■ ASSOCIATED CONTENT

Supporting Information

The Supporting Information is available free of charge at https://pubs.acs.org/doi/10.1021/acs.analchem.2c02223.

Materials, methods, detailed protocol of OBOC peptide library synthesis, HPLC of peptide, cell viability, detailed map of PLDs, cytotoxicity of W2 peptide, W2 peptide inhibits optical density, and CLSM images of W2 peptide inhibit pseudovirus infection (PDF)

■ AUTHOR INFORMATION

Corresponding Author

Weizhi Wang − *Key Laboratory of Medical Molecule Science and Pharmaceutics Engineering, Ministry of Industry and Information Technology, Key Laboratory of Cluster Science of Ministry of Education, Beijing Key Laboratory of Photoelectronic/Electro-photonic Conversion Materials, School of Chemistry and Chemical Engineering, Institute of Engineering Medicine, Beijing Institute of Technology, Beijing 100081, PR China;* orcid.org/0000-0002-7310-4068; Email: wangwz@bit.edu.cn

Authors

Shang Wu − *Key Laboratory of Medical Molecule Science and Pharmaceutics Engineering, Ministry of Industry and Information Technology, Key Laboratory of Cluster Science of Ministry of Education, Beijing Key Laboratory of Photoelectronic/Electro-photonic Conversion Materials, School of Chemistry and Chemical Engineering, Institute of Engineering Medicine, Beijing Institute of Technology, Beijing 100081, PR China*

Limin Zhang − *Key Laboratory of Medical Molecule Science and Pharmaceutics Engineering, Ministry of Industry and Information Technology, Key Laboratory of Cluster Science of Ministry of Education, Beijing Key Laboratory of Photoelectronic/Electro-photonic Conversion Materials, School of Chemistry and Chemical Engineering, Institute of Engineering Medicine, Beijing Institute of Technology, Beijing 100081, PR China*

Complete contact information is available at: https://pubs.acs.org/10.1021/acs.analchem.2c02223

Funding

The authors are grateful for financial support from the National Natural Science Foundation of China (22074006), the Beijing Natural Science Foundation (2222029), the Beijing Institute of Technology Research Fund Program for Young Scholars, the Analysis & Testing Center of BIT and the Youth Science and Technology Research Fund.

Notes

The authors declare no competing financial interest.

■ REFERENCES

(1) Bedford, J.; Enria, D.; Giesecke, J.; Heymann, D. L.; Ihekweazu, C.; Kobinger, G.; Lane, H. C.; Memish, Z.; Oh, M.-D.; Sall, A. A.; Schuchat, A.; Ungchusak, K.; Wieler, L. H.; Strategic, W. H. O. *Lancet (London, England)* **2020**, *395*, 1015−1018.

(2) Lan, J.; Ge, J.; Yu, J.; Shan, S.; Zhou, H.; Fan, S.; Zhang, Q.; Shi, X.; Wang, Q.; Zhang, L.; Wang, X. *Nature* **2020**, *581*, 215−220.

(3) Walls, A. C.; Park, Y.-J.; Tortorici, M. A.; Wall, A.; McGuire, A. T.; Veesler, D. *Cell* **2020**, *181*, 281−292.

(4) Ziegler, C. G. K.; Allon, S. J.; Nyquist, S. K.; Mbano, I. M.; Miao, V. N.; Tzouanas, C. N.; Cao, Y.; Yousif, A. S.; Bals, J.; Hauser, B. M.; Feldman, J.; Muus, C.; Wadsworth, M. H., 2nd; Kazer, S. W.; Hughes, T. K.; Doran, B.; Gatter, G. J.; Vukovic, M.; Taliaferro, F.; Mead, B. E. *Cell* **2020**, *181*, 1016−1035.e19.

(5) Jin, Z.; Du, X.; Xu, Y.; Deng, Y.; Liu, M.; Zhao, Y.; Zhang, B.; Li, X.; Zhang, L.; Peng, C.; Duan, Y.; Yu, J.; Wang, L.; Yang, K.; Liu, F.; Jiang, R.; Yang, X.; You, T.; Liu, X.; Yang, X. *Nature* **2020**, *582*, 289−293.

(6) Xia, S.; Lan, Q.; Su, S.; Wang, X.; Xu, W.; Liu, Z.; Zhu, Y.; Wang, Q.; Lu, L.; Jiang, S. *Signal Transduct Target Ther* **2020**, *5*, 92.

(7) Edwards, A. M.; Baric Ralph, S.; Saphire Erica, O.; Ulmer Jeffrey, B. *Science* **2022**, *375*, 1133−1139.

(8) Gordon, C. J.; Tchesnokov, E. P.; Schinazi, R. F.; Götte, M. *J. Biol. Chem.* **2021**, *297*, 100770−100771.

(9) Zhong, L.; Zhu, L.; Cai, Z.-W. *JOAT* **2021**, *5*, 298−313.

(10) Yuan, Z.-C.; Hu, B. *JOAT* **2021**, *5*, 287−297.

(11) Han, Y.; Král, P. *ACS Nano* **2020**, *14*, 5143−5147.

(12) Yang, G.; Li, Z.; Mohammed, I.; Zhao, L.; Wei, W.; Xiao, H.; Guo, W.; Zhao, Y.; Qu, F.; Huang, Y. *Signal Transduct Target Ther* **2021**, *6*, 227.

(13) Chi, X.; Liu, X.; Wang, C.; Zhang, X.; Li, X.; Hou, J.; Ren, L.; Jin, Q.; Wang, J.; Yang, W. *Nat. Commun.* **2020**, *11*, 4528.

(14) Schoof, M.; Faust, B.; Saunders Reuben, A.; Sangwan, S.; Rezelj, V.; Hoppe, N.; Boone, M.; Billesbølle Christian, B.; Puchades, C.; Azumaya Caleigh, M.; Kratochvil Huong, T.; Zimanyi, M.; Deshpande, I.; Liang, J.; Dickinson, S.; Nguyen Henry, C.; Chio Cynthia, M.; Merz Gregory, E.; Thompson Michael, C.; Diwanji, D. *Science* **2020**, *370*, 1473−1479.

(15) Wang, T.; Fang, X.; Wen, T.; Liu, J.; Zhai, Z.; Wang, Z.; Meng, J.; Yang, Y.; Wang, C.; Xu, H. *J. Med. Chem.* **2021**, *64*, 14887−14894.

(16) Tetz, G.; Tetz, V. *Microorganisms* **2022**, *10*, 280.

(17) Wrapp, D.; Wang, N.; Corbett Kizzmekia, S.; Goldsmith Jory, A.; Hsieh, C.-L.; Abiona, O.; Graham Barney, S.; McLellan Jason, S. *Science* **2020**, *367*, 1260−1263.

(18) Du, Q.; Wang, S.; Wei, D.; Sirois, S.; Chou, K.-C. *Anal. Biochem.* **2005**, *337*, 262−270.

(19) Wang, W.; Wang, Z.; Bu, X.; Li, R.; Zhou, M.; Hu, Z. *Adv. Healthcare Mater.* **2015**, *4*, 2802−2808.

(20) Guo, M.; Zhang, L.; Tian, Y.; Wang, M.; Wang, W. *Anal. Chem.* **2021**, *93*, 8035−8044.

(21) Saito, A.; Irie, T.; Suzuki, R.; Maemura, T.; Nasser, H.; Uriu, K.; Kosugi, Y.; Shirakawa, K.; Sadamasu, K.; Kimura, I.; Ito, J.; Wu, J.; Iwatsuki-Horimoto, K.; Ito, M.; Yamayoshi, S.; Loeber, S.; Tsuda, M.; Wang, L.; Ozono, S.; Butlertanaka, E. P. *Nature* **2022**, *602*, 300−306.
(22) Garcia-Beltran, W. F.; St. Denis, K. J.; Hoelzemer, A.; Lam, E. C.; Nitido, A. D.; Sheehan, M. L.; Berrios, C.; Ofoman, O.; Chang, C. C.; Hauser, B. M.; Feldman, J.; Roederer, A. L.; Gregory, D. J.; Poznansky, M. C.; Schmidt, A. G.; Iafrate, A. J.; Naranbhai, V.; Balazs, A. B. *Cell* **2022**, *185*, 457−466.e4.

https://doi.org/10.1021/acs.analchem.2c02223
Anal. Chem. XXXX, XXX, XXX−XXX